Chapter 4
Graphene Quantum Dots, Graphene Non-circular n–p–n-Junctions: Quasi-relativistic Pseudo Wave and Potentials

H. V. Grushevskaya, G. G. Krylov, S. P. Kruchinin, and B. Vlahovic

Abstract In our work, we build an atomic-like GQD-model and look for a GQD pseudopotential barrier, which is given by a set of well pseudopotentials for individual carbon atoms of the GQD. Numerical modelling of large-size GQDs has been performed in hydrodynamic approximation. It has been shown that pseudopotential removes degeneracy of energy levels for GQD-supercell and localizes valent electrons of the GQD-model on holes of n–p–n graphene-junction. Non-spherical symmetry of GQD wave functions leads to lifting of spin and valley degeneracy.

Keywords Graphene quantum dots · Graphene non-circular n–p–n-junctions · GQD-model · GQD pseudopotential barrier

4.1 Introduction

Nanoscale graphene quantum dots have the form of a quasicircle with a radius in the range from 3 [1] to 10 nm [2]. The parabolic confinement potential well has been used to calculate energy levels of a non-relativistic quantum dot [3–6]. But the results of such simulations describe only the low-lying part of the dot energy spectrum correctly.

H. V. Grushevskaya (✉) · G. G. Krylov
Physics Department, Belarusian State University, Minsk, Belarus
e-mail: grushevskaja@bsu.by

S. P. Kruchinin
Bogolyubov Institute for Theoretical Physics, Kiev, Ukraine

B. Vlahovic
North Carolina Central University, Durham, NC, USA

J. Bonča, S. Kruchinin (eds.), *Nanostructured Materials for the Detection of CBRN*,
NATO Science for Peace and Security Series A: Chemistry and Biology,
https://doi.org/10.1007/978-94-024-1304-5_4

In the paper [8] using the scanning tunnelling microscope (STM) it has been managed to form large quantum dots of the type of circular n−p−n and p−n−p junctions of graphene with a radius of about $r_{\text{dot}} \sim 100\,\text{nm}$ and atomic-like distribution of the electron density has been established. In such an approach the equivalence has been assumed on the change of the problem of motion of holes and electrons in the potential well $(-\kappa r^2)$ and $(+\kappa r^2)$ respectively, to the problem on scattering by the barrier $(-\kappa r^2)$ and $(+\kappa r^2)$ for electrons and holes respectively with a sufficiently high repulsive potential at the distance L far from the boundary of the quantum point so that $L \gg r_{\text{dot}}$. Naive considerations of the equivalence of such a change lead to the following unpleasant feature of the model as an appearance of false hole states (spurious states) at $r = 0,\ L$ (see section "Methods" in [8]) stipulated by the effective infiniteness of the well that is not a good choice for any Dirac problem. Usage of massless Dirac equation with a finite height step-like radial positive potential (barrier for electrons and well for holes) allows to perform correct relativistic simulations of electron density in the circular graphene n−p−n-junctions of the sizes 5.93 and 2.76 nm [1]. Despite the roughness of such calculations in comparison with the parabolic barrier, the theory and experiment should approximately coincide or, at least, qualitatively coincide if the assumption is valid on formation of a circular n−p−n-junction by mean addition of the step barrier to Dirac cone. But the relativistic simulation results satisfactory describe the only high energy level of the graphene quantum dots (GQDs), and the divergence between theoretical results and experimental data grows with the increase of GQD radius. Thus, relativistic barrier GQD models turn out to be inappropriate in the low-energy limit, and conversely, non-relativistic GQD models with a potential well do not work well in the high-energy limit.

Theory and experiment can be directly compared near graphene QD center and for following cases only: a scanning tunneling microscope (STM) tip radiuses r_{tip} are more than 70 nm or less than 20 nm. Electrically confining potentials have Gaussian shape for $r_{\text{tip}} \leq 20\,\text{nm}$ [7, 10]. The tight binding calculations (TB) in this case [8, 9] are applicable to the description of the behavior of wave functions in a QD-center only. Electrically confining potentials have cos-shape for $r_{\text{tip}} \geq 70\,\text{nm}$ [10]. Tight binding calculations (TB) in this case are applicable for the description of the wave functions in a QD center only. At present, there are no satisfactory methods for calculating GQDs and GQDs of large sizes.

In our work, we propose an atom-like GQD-model and look for a GQD pseudopotential barrier, which is given by a set well of potentials for distinct carbon atoms of the GQD.

4.2 An Atom-Like Model of Graphene Quantum Dot

A graphene quantum dot, consisting of N_{dot} carbon atoms is show schematically in Fig. 4.1a. Let a model GQD be considered as a "large atom" whose core i-th electrons are p_z-electrons of j-th C atoms, $j \neq i$. k-th p_z-electron of k-th C atom

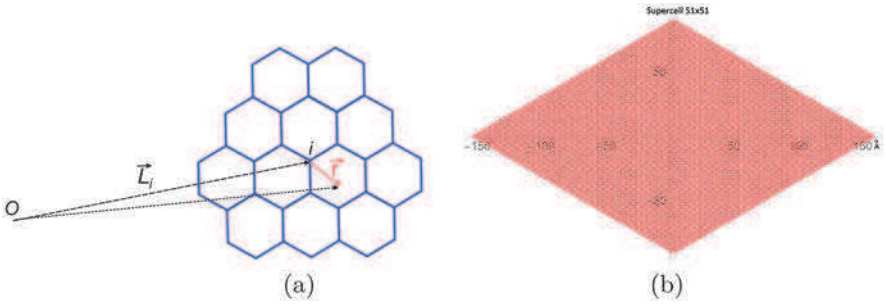

Fig. 4.1 (**a**) Scheme of graphene quantum dot: i-th atom C of GQD is located at i-th site with radius vector $\mathbf{L}_i$, and $\mathbf{r}$ is a radius vector of p_z-electron on respect to i-th lattice site. O is a reference point. (**b**) Graphene quantum dot super-cell from 51×51 primitive cells (100×150 Å)

plays a role of an external valent electron. Let k-th C atom is place in the lattice site with a radius-vector $\mathbf{L}_k$. The radius vector $\mathbf{r}$ will be calculated on respect to nearest lattice site and is a radius vector of the electron in an atom. Radius vector $\mathbf{X}_k$ of the valent electron of k-th atom reads $\mathbf{X}_k = \mathbf{L}_k + \mathbf{r}$.

Model graphene quantum dot has been constructed in the following way. Graphene primitive cell has basic vectors $\mathbf{b}_1 = a(3/2, \sqrt{3}/2), \mathbf{b}_2 = a(3/2, -\sqrt{3}/2)$ and two atoms (A and B) in the cell. Here a is the length of sp^2-hybridized C-C bond. We construct a supercell of the same symmetry type consisting of $(2n_1 + 1)(2n_2 + 1)$ primitive cells for $n_1 = 25, n_2 = 25$, that is shown in Fig. 4.1b.

Electronic band structure simulations in folding zone approximation gives the following set of eigenenergies $\pm\epsilon_{L_k}(q_i)$ and eigenstates $\psi_i^{(0)}(\mp q_i, \mathbf{r} + \mathbf{L}_k) = e^{\mp i\mathbf{q}_i\cdot(\mathbf{r}+\mathbf{L}_k)}u(\mathbf{r} + \mathbf{L}_k)$ for quasi-particle excitations of GQD:

$$\left\{\pm\epsilon_{L_k}(q_i),\ \psi_{L_k}^{(0)}\left(\mp\boldsymbol{q}_i, \mathbf{r} + \mathbf{L}_k\right)\right\}_{i,k=1,\ldots,N_{\mathrm{dot}}}, \tag{4.1}$$

where $\mathbf{q}_i$ is the wavevector of i-th quasi-particle located in k-th lattice site, upper sign "+" is related to electrons and lower to "−" corresponds to holes.

Now, let us construct the pseudopotential for atoms C in GQD.

4.3 Pseudo-potentials for Atoms C in Quantum Dot

Let us consider n−p−n-junction. Fock operator describing non-paired valent electron in many-electron system can not be considered as a Hamiltonian one [11]. But the procedure of the secondary quantization restore the Hamiltonian property

of the many-electron system by adding the operator of the "hole" $\hat{\epsilon}^{\dagger}$ to the Hartree-Fock Hamiltonian of m-th electron, scattering at a point $\mathbf{r}_i$ [12]:

$$\left[H(\mathbf{r}_i) + \hat{V}^{sc}(x_i) - \hat{\Sigma}^{x}(x_i)\right]\psi_m(x_i) = \left(\epsilon_m^{(0)} - \sum_{j=1}^{n}\hat{\epsilon}^{\dagger}P_j\right)\psi_m(x_i), \tag{4.2}$$

where $\hat{V}^{sc}(x_i)$ and $-\hat{\Sigma}^{x}(x_i)$ are operators of the Coulomb and exchange interactions respectively; $H(\mathbf{r}_i)$ is one-particle Hamiltonian without taking into account inter-electronic interactions, $\epsilon_m^{(0)}$ is an eigenvalue of $H(\mathbf{r}_i)$, $x_i = \{\mathbf{r}_i, \sigma_i\}$, σ_i is the spin of i-th electron, P_j is a projection operator, n is a number of electrons in a system.

Let us suppose that in the representation where the operator $\hat{\epsilon}^{\dagger}$ is a diagonal one, i-th electron with a radius-vector $\mathbf{L}_k + \mathbf{r}$ has been scattered on k-th atom with appearance of i-th hole with momentum $\mathbf{q}$, $i \neq k$ at Klein tunneling in the vicinity of the site with radius-vector $\mathbf{L}_k$. In this representation Eq. (4.2) is written as

$$\left[H(\mathbf{r}_i) + \hat{V}^{sc}(q\,x_i) - \hat{\Sigma}^{x}(q\,x_i)\right]\psi_m(q\,x_i) = \left(\epsilon_m^{(0)} - \sum_{j=1}^{n}\hat{\epsilon}^{\dagger}P_j\right)\psi_m(q\,x_i), \tag{4.3}$$

where $\hat{\epsilon}^{\dagger} = \tilde{\epsilon}_i(q)\hat{I}$, $\hat{I}$ is an operator unity in non-relativistic case or the identity matrix σ_0 for the Dirac equation. The inverse Fourier transformation

$$V_{i,L_k}(\mathbf{r})\psi_m(x_i) = \int e^{i\mathbf{q}\cdot(\mathbf{r}+\boldsymbol{L}_k)}\tilde{\epsilon}_i(q)\sigma_0\psi_m(q\,x_i)d\mathbf{q} \tag{4.4}$$

gives a nonrelativistic scattering potential. After calculating (4.4) we get

$$V_{i,L_k}(\mathbf{r}) = -2\pi\epsilon_{L_k}(q_i)\Theta\left(q_i - \frac{2\pi}{r}\right)\sigma_0 = -2\pi\epsilon_{L_k}(q_i)\Theta\left(\lambda_i - r\right)\sigma_0, \quad i \neq k; \tag{4.5}$$

where $q \to 0$, $r \leq a$, $\lambda_i = \frac{2\pi}{q_i}$. The potential (4.5), some well-known model potentials and a potential reconstructed based on experimental data are shown in Fig. 4.2. For a finite set of eigenenergies $\epsilon_{L_k}(q_i)$ the potential results to some staircase like potential which resemble the experimental one shown in Fig. 4.2b.

Further, a correct quasi-relativistic approximation of the pseudopotential for a graphene quantum dot will be constructed, and calculations of the valence orbitals of GQD will be performed based on the pseudopotential method.

Appearing after scattering of an electron on an atom hole with momentum $\mathbf{q}_i$ and radius-vector $\mathbf{L}_k + \mathbf{r}$ is always "frozen" in the vicinity of some lattice site with radius-vector $\mathbf{L}_k$. Due to the fact that such i-th hole together with electron belongs to

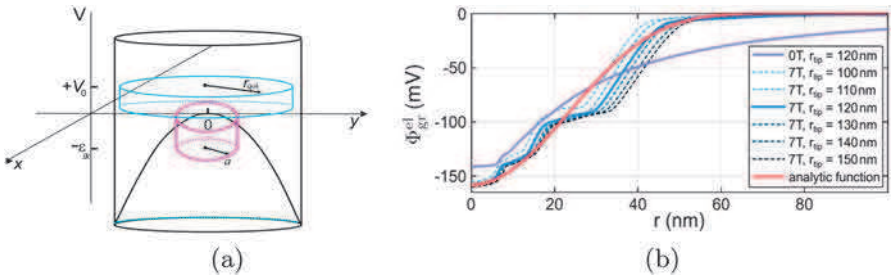

Fig. 4.2 (**a**) Model scattering potentials for the quantum dot (n–p–n junction): a circular well pseudo-potential $V_{i,L_k} = -\epsilon_{L_k}(q_i)\Theta\,(\lambda_i - r) \leq 0$ of the "frozen" atom with a size a (red curves); parabolic potential $(-\kappa r^2)$ with a large repulsive potential outside the graphene quantum dot [8] (black curves); a circular barrier potential $V = +V_0\Theta(r_{\rm dot} - r) \geq 0$ of radius $r_{\rm dot}$, $V_0 > 0$ (blue curves) see e.g., [13] and references therein. (**b**) Reconstructed potential based on experimental data of [9]

"frozen" k-th atom, $i \neq k$, so in some sense internal "core" electron of the atom-like model GQD gains some additional binding energy of the electron-hole pair. Binding energy for every core electron is given by the set of quasi-particle energies (4.1). In the atom-like model GQD the valent electron is k-th electron which is scattered (binds) on its own k-th atom C. The valent electron is described by (4.3) in an approximation of the frozen core. In the approximation of the frozen core, matrix elements ϵ_{kc} of the hole energy operator $\hat{\epsilon}^{\dagger}$, $c \neq k$ is approximately defined by the difference between the energy level of k-th atom C with valent GQD-electron and energy levels of c-th atoms C with core GQD-electrons:

$$\epsilon_{kc} = \left[E_k^{(0)} - E_c^{(0)}\right], \quad c \neq k, \tag{4.6}$$

where $E_k^{(0)}$ is the energy of the valent electron, $E_c^{(0)}$ are eigenvalues of the equation

$$\left[H_{D,c} + V_{c,L_k}(\mathbf{r})\right]\psi_c(\mathbf{r} + \mathbf{L}_k) = E_c^{(0)}\psi_c(\mathbf{r} + \mathbf{L}_k), \quad c \neq k. \tag{4.7}$$

To get $E_k^{(0)}$, it is necessary to write down the equation for eigenvalues and eigenfunctions for valent electron

$$H_{D,k}\psi_k(\mathbf{r} + \mathbf{L}_k) + \sum_{c \neq k} \epsilon_{kc} P_c \psi_k(\mathbf{r} + \mathbf{L}_k) = \epsilon_m^{(0)}\psi_k(\mathbf{r} + \mathbf{L}_k). \tag{4.8}$$

Operator $\sum_{c \neq k} \epsilon_{kc}\psi_c(\mathbf{r} + \mathbf{L}_k)$ entering into (4.8) is a QDT pseudo-potential. The solution of the Eq. (4.8) can be obtained by the successive approximations/ In zero

approximation we account of small differences between $\left[E_k^{(0)} - E_c^{(0)}\right]$, $k \neq c$: $\left[E_k^{(0)} - E_c^{(0)}\right] \approx \epsilon_m$ for the frozen core. Here ϵ_m is a constant. Then due to the arbitrariness of the zero energy point we assume $\epsilon_m = \epsilon_m^{(0)}$ and (4.8) is rewritten as

$$H_{D,k}\psi_k(\mathbf{r}+\mathbf{L}_k) = \epsilon_m^{(0)}\left[\psi_k(\mathbf{r}+\mathbf{L}_k) - \sum_{c\neq k}\epsilon_{kc}P_c\psi_k(\mathbf{r}+\mathbf{L}_k)\right]. \tag{4.9}$$

Let us designate the expression

$$\left[\psi_k(\mathbf{r}+\mathbf{L}_k) - \sum_{c\neq k}P_c\psi_k(\mathbf{r}+\mathbf{L}_k)\right] \tag{4.10}$$

through $\psi_{v,L_k}^{(0)}(\mathbf{r}+\mathbf{L}_k)$. It and (4.9) define a zero-order approximation for valent orbital

$$H_{D,k}\psi_{v,L_k}^{(0)}(\mathbf{r}+\mathbf{L}_k) = E_k^{(0)}\psi_{v,L_k}^{(0)}(\mathbf{r}+\mathbf{L}_k). \tag{4.11}$$

Substituting eigenvalues $E_k^{(0)}$ of (4.11) into (4.8), we find the equation for eigenfunctions and energy levels of k-th electron for

$$H_{D,k}\psi_k(\mathbf{r}+\mathbf{L}_k) + \sum_{c\neq k}\epsilon_{kc}\psi_c(\mathbf{r}+\mathbf{L}_k) = E_k^{(1)}\psi_k(\mathbf{r}+\mathbf{L}_k). \tag{4.12}$$

Taking into account the equality $i\hbar\frac{\partial}{\partial t}\psi_k(\mathbf{r}+\mathbf{L}_k) = E_k^{(1)}\psi_k(\mathbf{r}+\mathbf{L}_k)$. Then, the set

$$\left\{H_{D,k}\psi_k(\mathbf{r}+\mathbf{L}_k) + \sum_{c\neq k}\epsilon_{kc}\psi_c(\mathbf{r}+\mathbf{L}_k) = E_k^{(1)}\psi_k(\mathbf{r}+\mathbf{L}_k)\right\}_{k=1,r\to a}^{N_{qdots}} \tag{4.13}$$

can be considered in the continuous limit (hydrodynamic limit) $|\mathbf{L}_{k+1} - \mathbf{L}_k| \to 0$. Since the energy of electrons in the sites differs on the energy of quasi-particle excitation $\epsilon_{kc} = \epsilon_{c_i}$, Eq. (4.13) describes an electron moving in GQD:

$$\begin{aligned}\left\langle \mathbf{R}_{\text{qdot}}\right| H_D^{\text{qdot}}\left|\Psi_v^{\text{qdot}}\right\rangle + \sum_{i=1,c_i\neq v}^{N_{\text{dot}}-1}\epsilon_{c_i}(\mathbf{R}_{\text{qdot}})\left\langle \mathbf{R}_{\text{qdot}}\right|\Psi_{c_i}^{\text{qdot}}\left\rangle\right\langle\Psi_{c_i}^{\text{qdot}}\left|\Psi_v^{\text{qdot}}\right\rangle \\ = E_v^{\text{qdot}}\left\langle \mathbf{R}_{\text{qdot}}\right|\Psi_v^{\text{qdot}}\left\rangle.\end{aligned} \tag{4.14}$$

Here

$$V_{\mathrm{GQD}} = \sum_{i=1, c_i \neq v}^{N_{\mathrm{dot}}-1} \left|\Psi_{c_i}^{\mathrm{qdot}}\right\rangle \epsilon_{c_i}(\mathbf{R}_{\mathrm{qdot}}) \left\langle\Psi_{c_i}^{\mathrm{qdot}}\right| \tag{4.15}$$

is a GQD pseudopotential,

$$\left\langle\Psi_{c_i}^{\mathrm{qdot}}\right| \Psi_v^{\mathrm{qdot}}\right\rangle = \int \left\langle\Psi_{c_i}^{\mathrm{qdot}}\right| \mathbf{R}'_{\mathrm{qdot}}\right\rangle \left\langle\mathbf{R}'_{\mathrm{qdot}}\right| \Psi_v^{\mathrm{qdot}}\right\rangle \, d\mathbf{R}'_{\mathrm{qdot}}$$

is a scalar product, respectively, of these wave-functions $\left|\Psi_{c_i}^{\mathrm{qdot}}\right\rangle$ and $\left|\Psi_v^{\mathrm{qdot}}\right\rangle$ of core and valent electrons of GQD:

$$\left\langle\mathbf{R}_{\mathrm{qdot}}\right| \Psi_j^{\mathrm{qdot}}\right\rangle \equiv \Psi_j^{\mathrm{qdot}}(\mathbf{R}_{\mathrm{qdot}}) \in \left\{\psi_{L_k}^{(0)}\left(\mp\mathbf{q}_j, \mathbf{r}+\mathbf{L}_k\right)\right\}_{k=1,\ r=a}^{N_{\mathrm{qdot}}}, \tag{4.16}$$

$\epsilon_{c_i}(\mathbf{R}_{\mathrm{qdot}}) \in \left\{\pm\epsilon_{L_k}(q_i)\right\}_{k=1,\ldots,N_{\mathrm{dot}}}$; $\psi_{L_k}^{(0)}(\mp\mathbf{q}_i, \mathbf{r}+\mathbf{L}_k)$ and $\pm\epsilon_{L_k}(q_i)$ belong to the set (4.1), and for the valence electron the latter are an eigenvalue and a wave function for the same folding zone, and for the core electron they belong to different folding zones.

4.4 Simulation Methods

Quantization conditions can be obtained by "folding zones" applied in both directions allowing by quantum-dot symmetry. The quantization condition for the collective excitation with a wave-vector $\mathbf{k} = (k_x, k_y)$ for graphene nanotube with a chiral vector $\mathbf{C}$ reads

$$\mathbf{k} \cdot \mathbf{C} = 2\pi m, \quad m = 0, 1, \ldots, N. \tag{4.17}$$

Analogous, for the quantum dot we have to choose the following vectors as the basis vectors $\mathbf{C}_1 = (2n_1+1)\mathbf{b}_1$, $\mathbf{C}_2 = (2n_2+1)\mathbf{b}_2$ of the supercell, this results to the following systems for quantized wavevectors

$$\begin{aligned} (2n_1+1)\mathbf{b}_1 \cdot \mathbf{k} &= 2\pi m_1, \quad m_1 = 0, 1, \ldots, N; \\ (2n_2+1)\mathbf{b}_2 \cdot \mathbf{k} &= 2\pi m_2, \quad m_2 = 0, 1, \ldots, N, \end{aligned} \tag{4.18}$$

where N^2 is a number of $\pi(\mathrm{p}_z)$-electrons. Discrete set of energies is indexed by two integers m_1, m_2 and is based on graphene energy band spectrum $\epsilon(\mathbf{k})$. The last is used to find a distance from $\mathbf{k}_{mn} = (k_m, k_n)$ to a nearest Dirac point for a given

$m,\ n$. As a graphene model we use the earlier developed quasi-relativistic one in q^4 approximation for the exchange interactions (see detail in [14, 15]). The massless Dirac fermion model for graphene band structure is known to be good enough as a low energy excitations description up to 1 eV. For the quantum dot we have to work with the whole rather than the first Brillouin zone. This means accounting the **k** aside the Dirac cone apex in such a way to choose the nearest K-point used for energy evaluation. As an initial wave functions set for graphene quantum dot model we use the N^2 plane waves with appropriate $\mathbf{k}_{ij}$ and construct the lattice representation of this set in accord with the quantization condition (4.18). Spinor component of the waves are constructed as solutions of the appropriate Dirac-like equation within the framework of the graphene model [15].

Quantum Mechanics perturbation theory for non-orthogonal eigenfunctions sets should been used. Non-perturbed problem for the system (4.14) reads

$$H_0 \left|\psi_i^{(0)}\right\rangle = E_i^{(0)} \left|\psi_i^{(0)}\right\rangle \tag{4.19}$$

where the energy is determined as $E_i = E_i^{(0)} + \Delta E_i$. The solution of the perturbed problem

$$(H_0 + V)\ |\psi_i\rangle = E_i\ |\psi_i\rangle \tag{4.20}$$

for the state $|\psi_i\rangle$ is sought as a series on unperturbed eigenstates $\left|\psi_i^{(0)}\right\rangle$ in the form

$$|\psi_i\rangle = \sum_k c_{ik} \left|\psi_k^{(0)}\right\rangle. \tag{4.21}$$

After substitution (4.21) into (4.20) one gets

$$(H_0 + V) \sum_k c_{ik} \left|\psi_k^{(0)}\right\rangle = (E_i^{(0)} + \Delta E_i) \sum_k c_{ik} \left|\psi_k^{(0)}\right\rangle. \tag{4.22}$$

Scalar multiplying both sides of the last equation on $\langle\psi_m|$ and simplifying we get the generalized eigenvalue problem

$$\sum_k c_{ik} \left(V_{mk} - \Delta E_i\, S_{ij}\right) = 0 \tag{4.23}$$

where $V_{mk} = \left\langle\psi_m^{(0)}\right| V \left|\psi_k^{(0)}\right\rangle$, $S_{ij} = \langle\psi_i|\psi_j\rangle$ is the overlapping integral. The eigenenergies are given by

$$\mathrm{Det}\left(\hat{V} - \Delta E\, \hat{S}\right) = 0. \tag{4.24}$$

Simulations with pseudopotential (4.15) has been performed for lowest 40 levels. First order corrections for the energies and wave functions have been calculated.

4.5 Numerical Results and Comparison with Experiment for Electrostatically Confined QDs in Monolayer Graphene

Comparison of two spectra, initial one and the first perturbation theory results are shown in Fig. 4.3. As one can see, the perturbed spectrum is represented by five bands. Lowest one is a very narrow and consists of ten very near placed lines. Index of eigenstate, wave numbers and calculated energy levels in the folding zone approximation are given in the first three columns of the Table 4.1. As one can see from the table, some levels are degenerated. The resulting energy levels for first

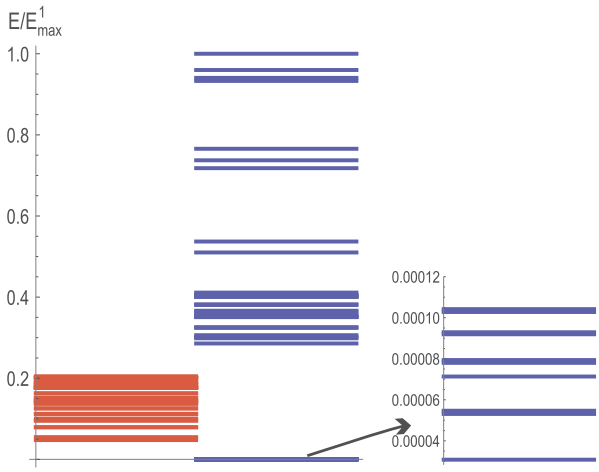

Fig. 4.3 Energy spectra for graphene quantum dot supercell from 51 × 51 primitive cells. Folding zone approximation (left); pseudo-potential approximation, first order perturbation theory result (right). Spectra are normalized on largest value of the right spectrum

Table 4.1 List of lowest eigenstates of the model graphene quantum dot

No.	$\mathbf{k}_i/\lvert K_A\rvert$	$E^{(0)}(\mathbf{k}_i)$, eV	$E_i^{(1)}$, eV
1	(0., –0.0522603)	0.682502	0.00044269
2	(0., 0.0522603)	0.787028	0.000762951
3	(–0.020115, –0.0871006)	**1.13688**	0.000785459
4	(0.020115, –0.0871006)	**1.13688**	0.00102502
5	(–0.020115, 0.0871006)	*1.37428*	0.00112078
6	(0.020115, 0.0871006)	*1.37428*	0.0011403
7	(0., –0.121941)	1.44642	0.00132088
8	(–0.04023, –0.121941)	**1.61086**	0.00133497
9	(0.04023, –0.121941)	**1.61086**	0.0014769
10	(–0.020115, –0.156781)	*1.80494*	0.00149691
11	(0.020115, –0.156781)	*1.80494*	4.10456

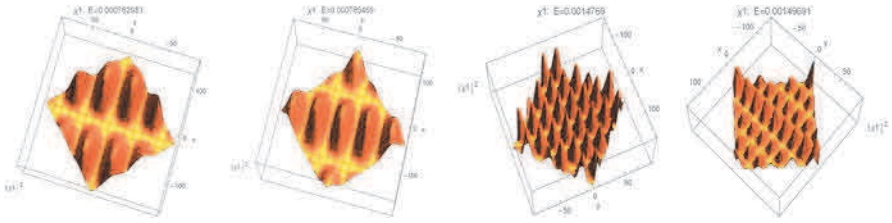

Fig. 4.4 Amplitude squares $|\chi|^2$ of strongly localized wave functions for different energy GQD-levels; energy values E are in insets to figures

order perturbation theory applied (again in sorted order) are shown in the fourth column of the Table 4.1. They already do not correspond to states with definite wave numbers $\mathbf{k}_i$ and are non-degenerated. Eigenfunctions for several lowest levels are shown in separate figures. As one can see electrons are localized on holes of n–p–n graphene junction. Figure 4.4 shows that every electron is confined by its hole but is not annihilated with it. Levels in Hartree–Fock approximations are ionization levels of the graphene QD.

The pseudopotential removes the degeneracy of the energy levels for the GQD-supercell and localizes the valent electrons of the GQD-model on the holes of the n–p–n graphene junction. Non-spherical symmetry of GQD wave functions in a magnetic field leads to lifting of spin and valley degeneration. Therefore, a tunneling current differential of the electrons pulled out from the holes by different electrical tip-induced fields yield more than 10 quadruplets of charging peaks for superlattice "graphene on boron nitride" in STM-experiments [9] Data in Table 4.1 and Fig. 4.3 with sign "–" are ten top hole levels of our n–p–n-junction model. These predicted by our model levels are very near in energy and are in the range from 0.00044269 to 0.00149691 eV. Their splitting in magnetic fields would explain the Coulomb staircase in the STM-experiments [9].

According to simulation results presented in Fig. 4.5a, b, there are weak localized energy levels, for example, with energies 0.00044269 and 0.00102502 eV, where electrons in GQD persist to be almost free. Thus, Klein paradox is absent in our model. Moreover, these weak localized states are wide ones that fit experimental data in Fig. 4.5c much better than theoretical curves in [8]. The weak localization explains the "tail" in distribution of hole density outside the quantum dot (see Fig. 4.5c). Besides, the presence of numerically revealed strongly localized GQD-states in Fig. 4.4 explains atomic-like distribution of electron density observed in STM-experiments [1, 8].

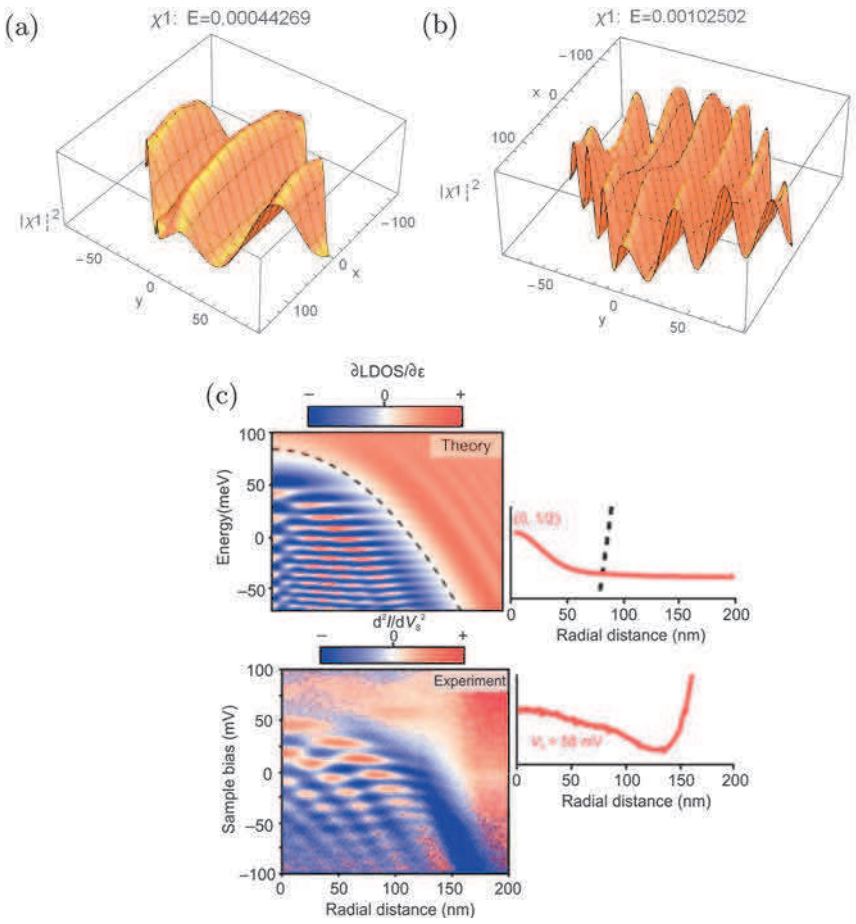

Fig. 4.5 Weak localized wave functions: amplitude square $|\Psi|^2$ for an energy GQD-level 0.00044269 (**a**) and 0.00102502 eV (**b**); (**c**) atom-like graphene QD with Gaussian potential: theory (up) and experiment (down) [8]

4.6 Conclusion

To summarize, the quasi-relativistic models of graphene n-p-n (p-n-p) junctions have been proposed. A supercell pseudopotential which electrically confines electrons (holes) in graphene quantum dot has been found. This potential has a finite depth.

References

1. Gutiérrez Ch, Brown L, Kim C-J, Park J, Pasupathy AN (2016) Klein tunnelling and electront rapping in nanometre-scale graphene quantum dots. Nat Phys 12:1069
2. Zhang J, Yu S-H (2016) Carbon dots: large-scale synthesis, sensing and bioimaging. Mater Today 19:382
3. Bogolubov NN, Soldatov NN, Kruchinin SP (2015) The theory of quantum dots in external magnetic field. Quantum Matter 4:352
4. Soldatov AV, Bogolyubov NN Jr, Kruchinin SP (2006) Method of intermediate problems in the theory of Gaussian quantum dots placed in a magnetic field. Condes Matter Phys 9(1):1
5. Repetsky SP, Vyshyvana IG, Molodkin VB, Kruchinin SP, Lizunov VV (2017) Influence of the adsorbed atoms of potassium on an energy spectrum of graphene. Metallofiz Noveishie Tekhnol 39:1017–1022
6. Kruchinin SP, Repetsky SP, Vyshyvana IG (2016) Spin-dependent transport of carbon nanotubes with chromium atoms. In: Bonca J, Kruchinin S (eds) Nanpmaterials for security. Springer, Dordrecht, pp 65–97
7. Giavaras G, Nori F (2012) Tunable quantum dots in monolayer graphene. Phys Rev B 85:165446
8. Lee J, Wong D, Velasco J Jr, Rodriguez-Nieva JF, Kahn S, Tsai H-Z, Taniguchi T, Watanabe K, Zettl A, Wang F, Levitov LS, Crommie MF (2016) Imaging electrostatically confined Dirac fermions in graphene quantum dots. Nat Phys 12:1032
9. Freitag NM, Chizhova LA, Nemes-Incze P, Woods CR, Gorbachev RV, Cao Y, Geim AK, Novoselov KS, Burgdörfer J, Libisch F, Morgenstern M (2016) Electrostatically confined monolayer graphene quantum dots with orbital and valley splittings. Nano Lett 16:5798
10. Maksym PA, Roy M, Craciun MF, Russo S, Yamamoto M, Tarucha S, Aoki H (2010) Proposal for a magnetic field induced graphene dot. J Phys Conf Ser 245:012030
11. Fock VA (1978) Fundamentals of quantum mechanics. MIR Publishing, Moskou
12. Krylova H, Hurski L (2013) Spin polarization in strongly correlated systems. LAP Lambert Academic Publishing. Saarbrücken, Germany
13. Kudryashov VV (2009) Exact wave functions of electron in a quantum dot with account of the Rashba spin-orbit interaction. Int J Nonlin Phen Compl Sys 12:199
14. Grushevskaya HV, Krylov G (2014) Quantum field theory of graphene with dynamical partial symmetry breaking. J Mod Phys 5:984
15. Grushevskaya HV, Krylov G (2015) Semimetals with Fermi velocity affected by exchange interactions: two dimensional Majorana charge carriers. Int J Nonlin Phen Compl Sys 18:266